

# Neutral Gas Expansion in a Cylindrical Helicon Discharge Chamber

S. Giannelli,\* A. Kieckhafer,† and M. L. R. Walker‡  
Georgia Institute of Technology, Atlanta, Georgia 30332

DOI: 10.2514/1.B34825

**The expansion of neutral gas in an open-ended cylindrical chamber into a large vacuum facility is investigated to understand neutral particle density distribution. The cylindrical chamber geometry with a single on-axis gas injection port is representative of a helicon plasma source discharge chamber. The neutral gas pressure profile along the cylinder wall is experimentally measured for argon and xenon mass flow rates of 0–200 sccm, at facility pressures up to  $3 \times 10^{-5}$  and  $3.8 \times 10^{-5}$  torr Ar and torr Xe, respectively. The average relative error between the experimentally measured pressure profiles and the numerical results obtained with a direct simulation Monte Carlo code is less than 10%, with the maximum relative error below 30%. The single on-axis injection port into the cylindrical discharge chamber results in a nonuniform neutral particle density distribution in the source due to the recirculation zone generated in the rear of the discharge chamber. This highlights the potential impact of the propellant injection system design on the neutral particle depletion phenomenon in helicon plasma sources.**

## I. Introduction

**I**N RECENT years, helicon discharges have attracted increasing interest not only in the areas of basic plasma physics research and plasma technology, but also in the electric propulsion community, the main applications being the helicon double-layer thruster (HDLT) [1] and the variable specific impulse magnetoplasma rocket (VASIMR) thruster [2,3]. Helicon waves are a bounded mode of whistler waves and are typically excited by RF power deposition along a dc magnetic field. The attractiveness of helicon sources comes from their efficiency as plasma generators and their simplicity in terms of system requirements. Plasma number densities on the order of  $10^{19}$ – $10^{20}$   $\text{m}^{-3}$  are attained at RF power levels of 1–2 kW (around two orders-of-magnitude higher than values achieved in inductively coupled sources of equivalent power), with ionization fractions close to 100% in the core of the source [4–7]. A “blue core” is observed in this mode of operation due to intense light emission from Ar II lines. Recent measurements on the VASIMR engine indicate values for the ionization cost 5–6 times higher than the theoretical ionization energy for several gases (Ar,  $\text{H}_2$ , Kr) [8,9]. In comparison, dc ionization mechanisms are known to require more than 10 times the theoretical ionization energy [6].

The physical structure of a helicon source typically consists of an insulating tube surrounded by an RF-driven antenna placed in a region with a relatively high (typically 500–1500 G) magnetic field parallel to the axis of the tube. In many helicon experiments for basic plasma research, the discharge chamber is composed of a small diameter (2–10 cm), relatively long (0.5–1.75 m) Pyrex® or quartz tube (aspect ratio, i.e., diameter-to-length ratio, between 0.03 and 0.2), with the exhaust end directly connected to a vacuum port. The facility backpressure is typically  $0.1$ – $20 \times 10^{-3}$  torr [4,6,10–17]. Because of

the physical geometry of this configuration, it is not possible to distinguish between facility pressure and the pressure inside the tube. In other configurations, the exit of the insulating tube is connected to an evacuated vacuum chamber of comparable or slightly larger size (most values of vacuum chamber-to-tube diameter ratio are much lower than 10) [18–25]. Experiments of propulsive interest usually involve the use of open-ended tubes of higher aspect ratio (typical values around 0.5) and require the entire helicon source (magnets, antenna, and insulating tube) to be placed inside a relatively large vacuum chamber (the ratio of chamber-to-tube diameter usually being 15–30) [26–28], so that the flow expands into a vacuum environment, which is representative of the on-orbit environment.

Although many areas of helicon source operation have been investigated, the role played by neutral particles and their distribution in the source (i.e., the way the neutral particles influence the operation and efficiency of the source) is not fully understood. Knowledge of the neutral particle evolution is especially important in helicon thrusters, because a uniform neutral particle density distribution is difficult to achieve in an open-ended high-aspect-ratio configuration. Here the terms “cold” and “hot” are used to refer to quantities before and after the RF power is turned on, respectively. The goal of this work is to highlight the importance of cold neutral particle dynamics by means of experimental and numerical simulations, to assess the effectiveness of the selected geometry of the tube and the feeding ports, to obtain a desired neutral particle distribution. The numerical simulations are validated with experimentally measured axial neutral pressure profiles along the wall of the insulating tube.

In Sec. II, we review recent investigations about the role played by the neutral particle distribution in the operation of helicon sources. In Sec. III, we describe the experimental apparatus employed for the wall pressure measurements, and in Sec. IV, the numerical direct simulation Monte Carlo (DSMC) code is described. Section V is devoted to the discussion of both the experimental and numerical results.

## II. Effect of Neutral Particle Density on Helicon Source Operation

The neutral particle density distribution within the discharge chamber of the helicon source affects both the ionization and ion acceleration processes: Ion production depends directly on electron-neutral collisions, and ion acceleration is impeded by ion-neutral collisions. The neutral particle distribution inside the tube, with respect to the position of the RF antenna, strongly affects the deposition of power into the propellant gas and hence the plasma production and overall efficiency of the device [29]. Moreover, knowledge of the neutral particle density distribution within the

Received 14 October 2012; revision received 9 January 2013; accepted for publication 24 January 2013; published online 5 April 2013. Copyright © 2013 by Sebastiano Giannelli, Alexander Kieckhafer, Mitchell L.R. Walker. Published by the American Institute of Aeronautics and Astronautics, Inc., with permission. Copies of this paper may be made for personal or internal use, on condition that the copier pay the \$10.00 per-copy fee to the Copyright Clearance Center, Inc., 222 Rosewood Drive, Danvers, MA 01923; include the code 1533-3876/13 and \$10.00 in correspondence with the CCC.

\*Visiting Research Scholar; currently Ph.D. Candidate, Department of Aerospace Engineering, via G. Caruso 8, University of Pisa, 56122 Pisa, Italy. Student Member AIAA (Corresponding Author).

†Postdoctoral Researcher, High-Power Electric Propulsion Laboratory, Department of Aerospace Engineering, 270 Ferst Drive; currently ZIN Technologies, Cleveland, OH.

‡Associate Professor, High-Power Electric Propulsion Laboratory, Department of Aerospace Engineering, 270 Ferst Drive. Associate Fellow AIAA.

device will assist with the development of appropriate minimum facility pressure limits and understanding the importance of charge-exchange (CEX) collisions in the plume. Facility pressure and the impact of CEX collisions are known limiting factors in other high-specific-impulse devices such as ion and Hall-effect thrusters [30].

A well-known phenomenon that affects helicon source operation is “neutral pumping,” (i.e., the depletion of neutral particles from the core region of the source), which leads to limitations in the attainable plasma density and ionization efficiency [4,12,29,31–36]. Reductions in neutral particle density of one order of magnitude or more have been observed in the core of helicon discharges [4,12,36], both with respect to the cold flow values and between different regions in the source. Neutral pumping accounts for the emergence of different helicon modes [32], for nonmonotonic variation of plasma density with varying RF power [34], for electron species heating by limitation of RF power deposition into ionization [35], for the radial nonhomogeneity of plasma properties [33], and for the inception of discharge oscillations in connection to neutral particle ingestion in vacuum chambers [31]. Several mechanisms are thought to be behind the neutral pumping phenomenon: heating of neutral particle [4], which requires lower neutral density to preserve pressure balance in the source; neutral particle diffusion [12]; and “ion pumping,” that is, the diffusion of ionized atoms to the wall of the tube being much faster (because of presheath electric fields) than the diffusion of neutral atoms (generated by recombination) from the wall to the core of the plasma [33]. The neutral particle density can also directly influence ion acceleration in helicon thrusters, with important consequences on the propulsive effectiveness of these sources [37].

Previous direct measurements of the neutral particle density distribution were made with the discharge turned on, either by means of pressure gauges [12,33,38] (i.e., capacitive manometers or barometers) or by means of nonintrusive, laser-driven optical systems [39,40]. The uncertainty in neutral particle density measurements obtained with a pressure gauge within a plasma is large because the gauge cannot discriminate between neutral gas density depletion and neutral gas heating (i.e., the pressure in the nonisothermal gas present in an RF discharge depends on both the neutral particle density and temperature, so that a variation in the neutral pressure cannot be a priori related to a variation of the particle density). Moreover, the physical presence of the probe in the flow can strongly alter the original flow pattern. Spectroscopic approaches can measure the neutral gas temperature and overcome the limitations of the barometer measurements [41]. Spectroscopic techniques are based on the evaluation of the rotational temperature of a trace ( $\sim 5\%$  by mass) molecular gas, such as  $N_2$ , injected into the main feed gas. The translational temperature of the main feed gas is assumed to be equal to the rotational temperature of the trace molecular gas. However, the analysis of many of these optical measurements often requires the development of complex collisional-radiative models for the calculation of atomic excited states and the interpretation of the light collected from the plasma. These models can introduce significant uncertainty into neutral particle density measurements because of the uncertainties related to the description of the collisional and diffusive phenomena and to the detailed knowledge of the necessary physical properties, such as the dependence of the collisional cross sections as a function of particle temperatures (electron temperature, heavy species translational temperature, and rotational and vibrational temperature of molecular gases) [42].

The design of the propellant injection system is believed to play a major role in the neutral pumping phenomenon [29]. Although neutral pumping is strictly related to the plasma equilibrium configuration (as previously stated, it is strongly affected by neutral particle heating and ion diffusion), in this work, we focus our attention on the cold neutral particle density evolution in the discharge chamber, because it has a nonnegligible effect on the discharge equilibrium. Knowledge of the cold neutral particle density distribution in the source can be used to better understand the previously cited mechanisms of neutral depletion, as well as allow a propellant injection design that mitigates the neutral pumping effect and improves the overall operation of the helicon source. In addition, a simple and

reliable procedure to determine the cold neutral background flow is a valuable tool for design improvements.

### III. Experimental Apparatus

All tests were performed in vacuum test facility 1 (VTF-1) at the High Power Electric Propulsion Laboratory of the Georgia Institute of Technology, which is shown in Fig. 1a. The facility consists of a 4-m-diam by 7-m-long cylindrical stainless steel vacuum chamber. The facility is evacuated to a pressure of approximately  $1.5 \times 10^{-2}$  torr  $N_2$  by a pair of Oerlikon Leybold RA5001 roots pumps, capable of a combined pump rate of 3600 l/s. High vacuum is achieved through six 1.5-m-diam diffusion pumps, capable of a combined pump rate of 600,000 l/s on nitrogen, and a facility base pressure below  $1 \times 10^{-6}$  torr. Facility pressure is measured by two Varian 571 Bayard-Alpert ionization gauges, controlled by a Varian XGS-600 ion gauge controller. Uncertainty in the facility pressure measurements is approximately  $\pm 20\%$ . Argon and xenon gases are supplied by an MKS 1179A mass flow controller connected to an MKS 247 power supply/readout, with a combined accuracy of  $\pm 1\%$  of set point. The mass flow system was calibrated by observing the pressure rise in a 0.959 l calibration plenum and calculating mass flow from the pressure rise and physical properties of the gas.

Figure 1b shows a schematic of the cylindrical tube used for the pressure measurements, which is manufactured to similar dimensions as the HDLT [25]. The tube is fabricated from acrylic and is 29.2 cm long and 13.3 cm in diameter (inner wall). The helicon tube has 23 ports drilled in the wall at  $12.7 \pm 0.025$  mm intervals, which provide access to the pressure at the tube wall. Each port has a nylon tube with a self-sealing valve attached to it, so that gas cannot escape except when the pressure sensor is attached. The pressure sensor is an MKS model 626 Baratron pressure gauge with a maximum range of  $10^{-1}$  torr and an accuracy of  $\pm 0.5\%$ , connected to an MKS PDR2000 power supply and readout. The Baratron pressure gauge is mounted on a moveable arm with a vertical translation range of 50 mm, which allows the sensor to be lowered onto a port for measurement, then raised so that the Baratron pressure

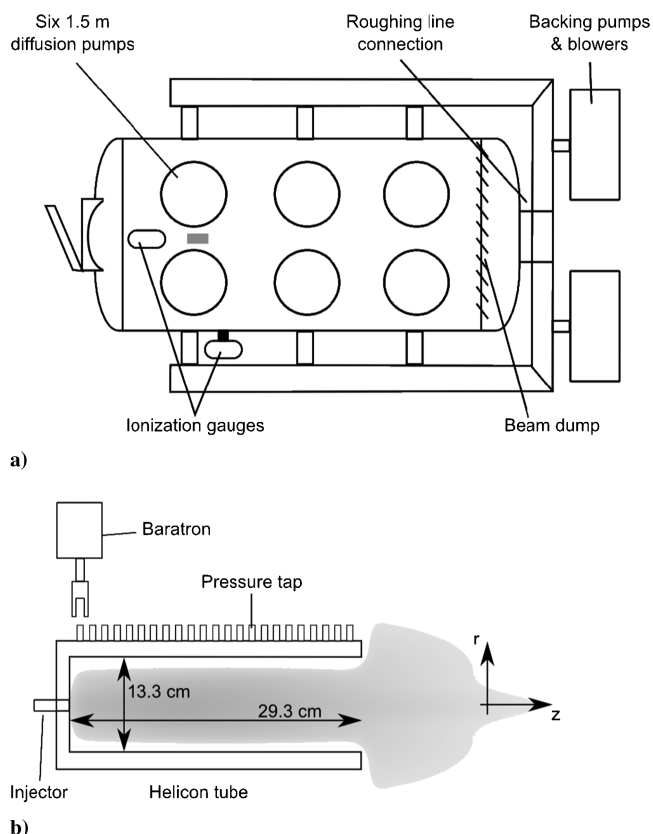


Fig. 1 Experimental apparatus: a) VTF 1 (helicon tube in gray), b) helicon tube setup.

gauge can be moved to another port by means of an automated Parker Daedal linear motion table. The pressure is measured along the wall to minimize perturbations to the neutral flow dynamics within the cylinder.

Pressure at the wall of the helicon tube is measured for argon and xenon at mass flow rates from 0 to 200 sccm (0 to  $\sim 5.98$  mg/s in argon; 0 to  $19.65$  mg/s in xenon) with increments of 25 sccm ( $\sim 0.75$  mg/s in argon;  $\sim 2.46$  mg/s in xenon). The VTF-1 facility reaches a steady pressure within 30 s of a change in mass flow rate. To move the Baratron pressure gauge between the pressure measurement wall ports, an arm first raises the pressure gauge to disengage it from the active port, the motion table then moves the Baratron pressure gauge to the next port, then the arm lowers the pressure gauge into the port until the self-sealing valve in the pressure port fitting opens. The Baratron pressure gauge reading is zeroed upon arrival at each wall port to avoid zero drift due to changes in the inclination of the sensor. At facility pressures less than the  $5 \times 10^{-5}$  torr, the minimum measurable pressure of the Baratron pressure gauge, the gauge reading is set to zero. At higher facility pressures, the Baratron pressure gauge reading is set to the facility pressure. The 95% confidence intervals for the pressure measurements, as calculated by the analysis of variance method, are  $\pm 7.0 \times 10^{-5}$  torr Xe and  $5.0 \times 10^{-5}$  torr Ar.

#### IV. Direct Simulation Monte Carlo Simulations

The use of hybrid DSMC–particle-in-cell (PIC) codes is well established in the electric propulsion (EP) community to investigate the performance of electric thrusters and the interaction of their plumes with spacecraft [43–47]. The DSMC method [48] is employed to model heavy particle collisions, whereas the PIC method models ion motions in electric fields [49]. DSMC codes, without the PIC portion, have also been employed to investigate the cold neutral flow from EP devices into large vacuum chambers [50,51], showing very good agreement with experimental data. This work uses the freely distributed two-dimensional DSMC code DS2V developed by Bird, which is widely used in research communities and takes advantage of recently developed advanced numerical techniques for DSMC calculations [52]. Simulation of collisions between particles is based on a modified version of the quantum vibration model, which allows for exact energy equipartition among the different energy modes [52]. Although proper chemical models are implemented, which take into account molecular dissociation and ionization (and the respective inverse reactions), in our case (given the nature of the simulated gases and the relatively low temperatures involved) only neutral particles are present. The flow in the cylindrical discharge tube is modeled as axisymmetric and only half of the  $r$ - $z$  plane is employed in the calculations. The symmetry axis is positioned on the lower boundary of the bounding rectangle of the computational domain. Preloaded specific gas models for argon and xenon were selected in the graphical interface of the code. The initial condition for our simulations is full vacuum. The simulations are complete when the number of particles in the computational domain reaches an asymptote and the wall pressure profile remains constant between two consecutive updates of the model output. Manual adjustments of the number of simulated molecules and adaption of cell size are performed during the calculations to ensure that the criterion for a good DSMC simulation (i.e., the ratio of the mean local separation between collision partners and the local mean free path being much lower than unity) is fulfilled [52]. The average number of simulated particles at steady state is  $1.2 \times 10^6$ , whereas the average number of collision cells is  $1.5 \times 10^5$ ; the time step is adaptively calculated by the code to satisfy the aforementioned criterion over the entire simulation domain.

Because the only datum for each simulation is the mass flow rate, we must set the inlet gas velocity or density to initiate the simulation. In general, the actual values may depend on many factors, which include feed system design, mass flow rate, helicon tube geometry, and facility backpressure. The feed system affects the inlet gas velocity because it causes a drop in pressure (both concentrated and distributed) between the exit of the propellant gas bottle and the inlet

to the discharge chamber due to the viscous effects in the feed lines. Mass flow rate directly affects the inlet velocity as very high mass flow rates will exhibit higher pressure drop at the inlet section between the region upstream of the injection port, where the gas flows from the pressurized bottle, and the region downstream of it, where the flow is directly affected by the evacuated facility pressure. On the other hand, very low mass flow rates can lead to transitional or even free molecular flow inside the feeding lines themselves. The geometry of the insulating tube of the helicon determines the dynamics of the gas expansion and diffusion from the inlet port, which determines the local value of the static pressure. System backpressure determines the downstream pressure in case of subsonic flows or the position and shape of the sonic boundary in case of sub-to-supersonic expansion. The choice of the inlet density or velocity has a strong effect on the results and is discussed later in the manuscript.

Given the high number of possible variables in the problem and the practical impossibility to take them into account in a reliable way, we chose to use one of the two inlet values (density and velocity) as a free parameter and to compare the wall pressure data obtained from the DSMC simulations with the experiments. Through iteration, we identify the value of the free parameter that gives the best agreement with the experimental values. Explicitly, best agreement is defined as the lowest global error, calculated as  $\sqrt{[\sum((p_{\text{exp}} - p_{\text{DSMC}})/p_{\text{exp}})^2]}$ , where  $p_{\text{exp}}$  is the measured value of the neutral pressure at the wall,  $p_{\text{DSMC}}$  is the corresponding value calculated with the DSMC code, and the sum is taken over all the measured experimental points on the tube wall. This procedure allows for a more precise comparison with the experimental data than assigning a priori a sonic condition at the inlet [50]. To make comparisons easier, given the different gases used, the inlet Mach number is taken as a variable parameter. As anticipated, the inlet conditions have a nonnegligible effect on the wall pressure profile, mainly in terms of absolute magnitude. As expected, a reduction in the inlet Mach number leads to an increase in the static wall pressure. Note that the flow inside the discharge chamber is subsonic. The inlet Mach number is iterated in 1/32 increments to obtain the flow solution. Greater accuracy in finding the inlet Mach number is possible, but 1/32 increments provide acceptable resolution of the inlet Mach number for the scope of this work.

Initially, simulations are performed within a computational domain with the same physical dimensions as the VTF-1. Diffuse reflection and full temperature accommodation are assumed at the chamber and tube walls.

The diffusion pumps are simulated as an interface with vacuum on the outer wall of the chamber. The axial extent of this interface is chosen so that its surface area is equal to the actual total surface of the pumps. This case is referred to as the large-volume case. Given the relatively high number of simulations required, an analysis of the sensitivity of the results to the computational domain dimensions is performed. A compromise between accuracy of the results and computational effort was to choose a computational domain that spans 2 m in the axial direction and 1 m in the radial direction, with all boundaries (but for the lower one coinciding with the symmetry axis of the flow) set as interfaces with vacuum. This case is referred to as the reduced-volume case.

#### V. Results and Discussion

This section validates the numerical results through comparison with the experimentally measured cold neutral wall pressure profile. The results of the simulation are then used to understand the neutral particle density distribution within the cylindrical helicon chamber.

Figure 2 shows a comparison of the wall pressure measurements in argon at 25 sccm mass flow rate, with the DSMC simulations both in the large- and reduced-volume cases. First, these plots give an example of the dependence of the simulated wall pressure on the inlet Mach number of the gas. As anticipated, higher inlet Mach numbers lead to lower average values of the wall pressure. In this case, the best agreement is found to be for an inlet Mach number of 6/32. The choice to employ a reduced computational domain is validated here because it does not have a large effect on the numerical results for the

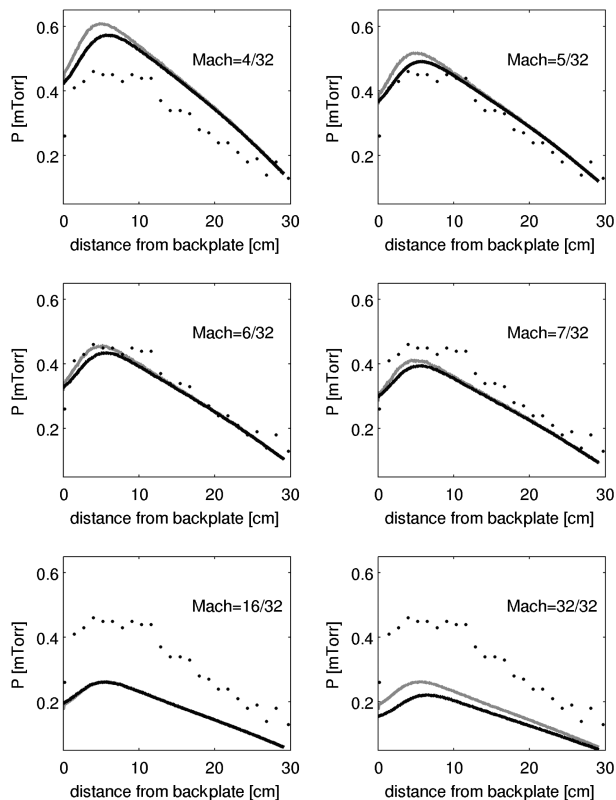


**Fig. 2** Experimental (dots) and numerical wall pressure: large (gray) and reduced (black) volume (25 sccm argon mass flow rate).

wall pressure (in the  $M = 0.5$  case, they are completely superimposed). The only noticeable differences between the large- and reduced-volume cases arise at the very first portion of the tube, which will be discussed later, and for the case of sonic inlet, which is very far from the measured values and thus not considered important. Results

for different mass flow rates both in argon and xenon exhibit the same qualitative properties.

Figures 3a and 3b show the experimental data and corresponding simulation results for all of the argon and xenon mass flow rates investigated. The agreement between the experimental data and simulation results is in general fairly good, with average relative error below 10% and local maximum error around 30% in the worst cases (mainly in the upstream region for argon simulations and at the downstream end of the channel for xenon simulations). For all the cases, the inlet Mach number giving the best agreement is around 5/32, even if in some cases an even more accurate choice of this parameter would lead to closer results with the experimental data, especially for some of the cases with xenon. A common pattern, which is both experimentally and numerically detected, is the fact that the cold neutral pressure at the wall is not at all constant, as would be desirable in terms of uniformity of the neutral background, nor monotonically decreasing, as would be expected from an expansion into vacuum, but peaks approximately 10 cm from the backplate. The reason is easily found by looking at Fig. 4, in which the streamlines in the first half of the channel are traced in the case of a 100 sccm argon flow rate (same qualitative result holds true in the other cases). The upper-left corner in the  $r-z$  plane is characterized by a large recirculating flow structure, which is responsible for the local lowering of the static pressure at the wall. The presence of this structure is likely due to the feed strategy: Injection of propellant through a central hole on the axis of the device does not allow for a smooth expansion of the flow in the tube, which reattaches at the wall only at a certain distance from the backplate. An important point to notice is that the qualitative behavior outlined here (i.e., the presence in the numerical data of a peak of the wall pressure distribution and of a recirculating flow structure near the inlet) is not dependent on the particular choice for the inlet Mach number, as demonstrated by Fig. 2.

Figure 5a shows the DSMC data for the axial variation of the neutral density along the axis of the tube, at a mass flow rate of 100 sccm of argon, for two different radial positions:  $r = 0$  cm (along the tube axis) and  $r = 6.65$  cm (along the inner wall of the tube). The axial neutral particle density profile decreases by more

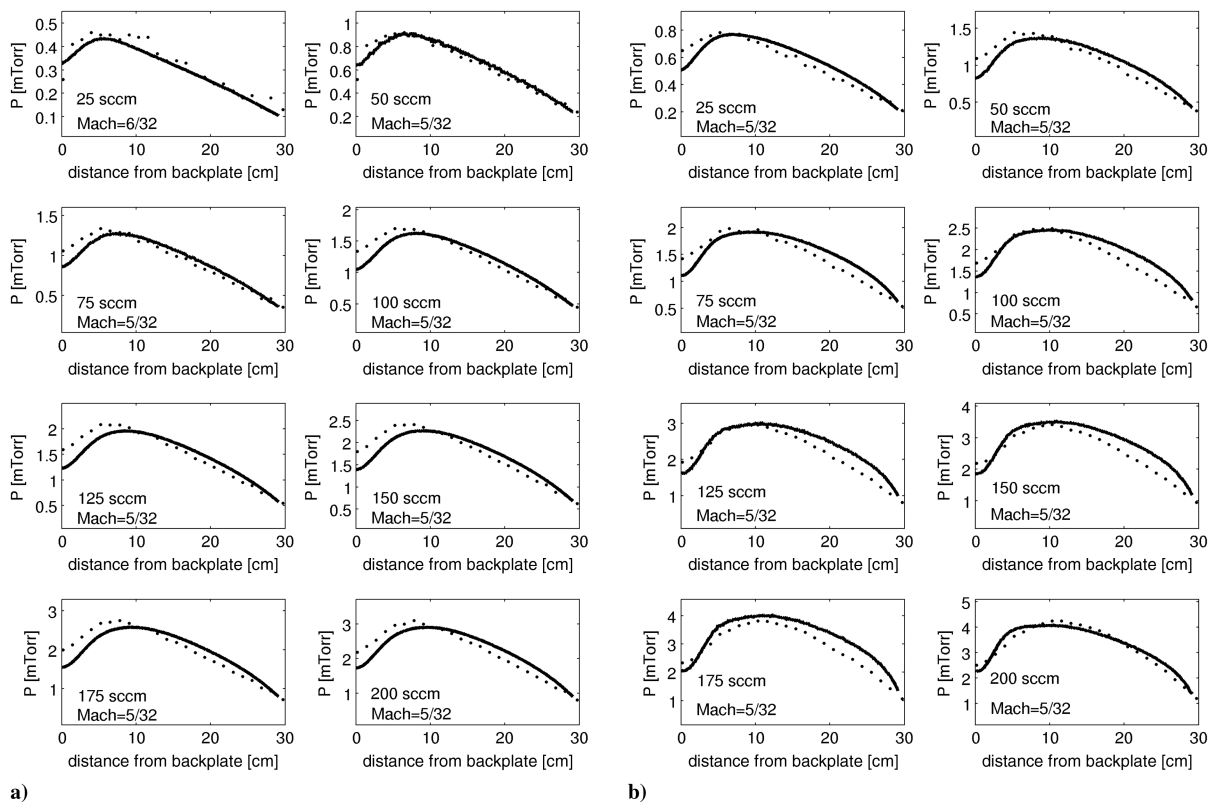


**Fig. 3** Experimental (dots) and numerical wall pressure (inlet Mach for best agreement): a) argon, b) xenon.

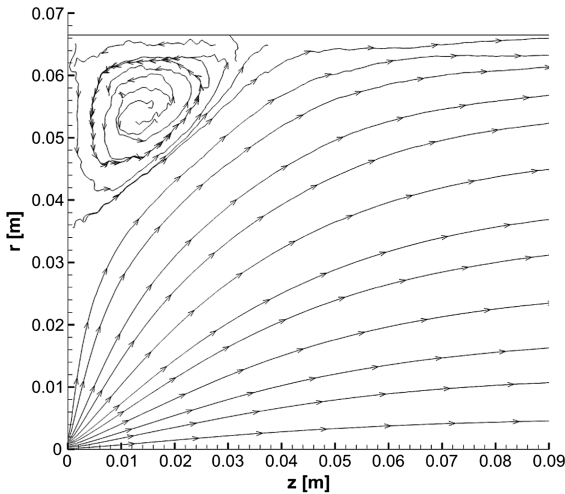
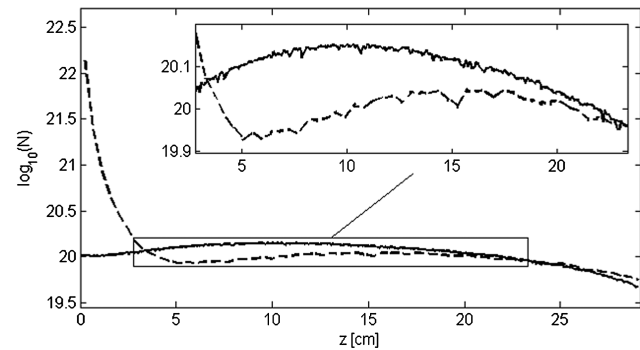


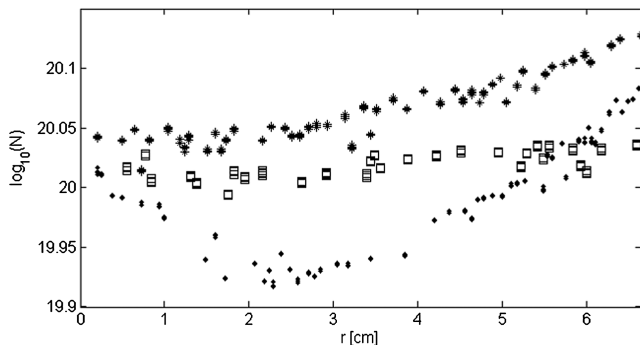
**Fig. 4** Streamlines in the upstream end of the helicon tube showing the presence of a recirculating flow structure (100 sccm argon mass flow rate).

than two orders of magnitude in the first 10 cm of the channel, due to the position of the injection port, whereas in the remaining downstream part of the channel, the neutral particle density distribution remains of the same order of magnitude, although not perfectly homogeneous nor monotonic. The axial neutral particle distribution in the vicinity of the wall is much more homogeneous, although not being monotonic.

Figure 5b shows the radial density profiles at three different axial positions:  $z = 4, 14,$  and  $23$  cm (i.e., near the exit plane). The mass flow rate is again 100 sccm of argon, but similar results hold for the other cases. The only position with an almost constant radial distribution of neutral particles is at  $z = 23$  cm. The  $z = 4$  cm position has a nonmonotonic concave variation of the density along the radius, the local peak on the axis being related to the vicinity of the



a)



b)

**Fig. 5** Neutral particle density distribution: a) axial on center-line (dots) and inner wall (dashes), b) radial at  $z = 4$  (dots),  $14$  (asterisks) and  $23$  cm (boxes).

injection port. The  $z = 14$  cm position also presents a concave, although monotonic, radial density profile. What is most interesting is that these results show that, given a particular geometrical configuration of the source, the cold neutral flow is characterized by neutral particle depletion in the center of the source, which is related to purely gas-dynamic reasons and not to the specific equilibrium configuration with the plasma discharge turned on. This is further illustrated by the zoomed plot in Fig. 5a, which clearly shows that, for most of the tube length, the neutral density on the axis of the device is lower than the density on the wall. We can infer that such a situation increases the detrimental effect of ion pumping and neutral diffusion, when the discharge is on, in terms of neutral particle depletion. The magnitude of the variation of the cold neutral density along the radius is indeed of the same order of the measured hot neutral particle depletion by other authors [33,38,40].

One possible way to reduce the observed nonhomogeneity could involve the adoption of a different injection system, such as a multihole plate that would allow for a more uniform injection over the whole backplate of the discharge chamber. Further optimization could be attained by measuring the effect of the improved design on the plasma equilibrium and iterating on the injection system design.

## VI. Conclusions

This work illuminates the impact of gas injection configuration on cold flow neutral dynamics within cylinders that exhaust into vacuum environments. The experimental conditions and simulations are representative of typical helicon plasma source operation. Direct Monte Carlo simulations, validated by experimental pressure measurements along the cylinder wall for several mass flow rates of argon and xenon gas, quantify the neutral particle distribution throughout the cylinder.

The results show that the neutral particle distribution is characterized by a concave neutral density distribution on the axis of the device, and so the single on-axis injection port does not achieve a uniform cold neutral particle distribution in the discharge chamber, at least for geometrical configurations (in terms of discharge chamber dimensions) typical of propulsive experiments of helicon plasma sources. It is possible that the observed nonhomogeneity of the neutral background flow contributes to the neutral particle depletion phenomenon when the helicon plasma discharge is turned on, although further and specific investigations are required to determine the eventual correlation between cold flow properties and the discharge equilibrium, possibly by testing different injection systems.

## References

- [1] Charles, C., Alexander, P., Costa, C., Sutherland, O., Boswell, R. W., Pfitzner, L., Franzen, R., Kingwell, J., Parfitt, A., Frigot, P. E., Gonzales del Amo, J., Gengembre, E., and Saccoccia, G., "Helicon Double Layer Thrusters," *International Electric Propulsion Conference*, IEPC Paper 2005-290, 2005.
- [2] Chang Diaz, F. R., "An Overview of the VASIMR Engine: High Power Space Propulsion with RF Plasma Generation and Heating," *American Institute of Physics Conference Proceedings*, Vol. 595, American Institute of Physics, Melville, NJ, 2001, pp. 3–15.
- [3] Squire, J. P., Chang-Diaz, F. R., Glover, T. W., Jacobian, V. T., McCaskill, G. E., Winter, D. S., Baity, F. W., Carter, M. D., and Goulding, R. H., "High Power Light Gas Helicon Plasma Source for VASIMR," *Thin Solid Films*, Vols. 506–507, 2005, pp. 579–582. doi:10.1016/j.tsf.2005.08.061
- [4] Boswell, R. W., "Very Efficient Plasma Generation by Whistler Waves near the Lower Hybrid Frequency," *Plasma Physics and Controlled Fusion*, Vol. 26, No. 10, 1984, pp. 1147–1162. doi:10.1088/0741-3335/26/10/001
- [5] Chen, F. F., "Plasma Ionization by Helicon Waves," *Plasma Physics and Controlled Fusion*, Vol. 33, No. 4, 1991, pp. 339–364. doi:10.1088/0741-3335/33/4/006
- [6] Chen, F. F., "Experiments on Helicon Plasma Sources," *Journal of Vacuum Science and Technology A*, Vol. 10, No. 4, 1992, pp. 1389–1401. doi:10.1116/1.578256
- [7] Chen, F. F., "Helicon Plasma Sources," *High Density Plasma Sources*, edited by Popov, O. A., Noyes Publ., Park Ridge, NJ, 1995, pp. 1–75.

- [8] Longmier, B. W., Cassady, L. D., Ballenger, M. G., Carter, M. D., Chang-Diaz, F. R., Glover, T. W., Ilin, A. V., McCaskill, G. E., Olsen, C., Squire, J. P., and Bering, E. A., "VX-200 Magnetoplasma Thruster Performance Results Exceeding Fifty-Percent Thruster Efficiency," *Journal of Propulsion and Power*, Vol. 27, No. 4, 2011, pp. 915–920.  
doi:10.2514/1.B34085
- [9] Longmier, B. W., Squire, J. P., Cassady, L. D., Ballenger, M. G., Carter, M. D., Olsen, C., Ilin, A. V., Glover, T. W., McCaskill, G. E., Chang-Diaz, F. R., Bering, E. A., and Del Valle, J., "VASIMR VX-200 Performance Measurements and Helicon Throttle Tables Using Argon and Krypton," *International Electric Propulsion Conference*, IEPC Paper 2011-156, 2011.
- [10] Chen, F. F., Sudit, I. D., and Light, M., "Downstream Physics of the Helicon Discharge," *Plasma Sources Science and Technology*, Vol. 5, No. 2, 1996, pp. 173–180.  
doi:10.1088/0963-0252/5/2/009
- [11] Blackwell, D. D., and Chen, F. F., "Two-Dimensional Imaging of a Helicon Discharge," *Plasma Sources Science and Technology*, Vol. 6, No. 4, 1997, pp. 569–576.  
doi:10.1088/0963-0252/6/4/015
- [12] Gilland, J., Breun, R., and Hershkowitz, N., "Neutral Pumping in a Helicon Discharge," *Plasma Sources Science and Technology*, Vol. 7, No. 3, 1998, pp. 416–422.  
doi:10.1088/0963-0252/7/3/020
- [13] Rayner, J. P., and Cheatham, A. D., "Helicon Modes in a Cylindrical Plasma Source," *Plasma Sources Science and Technology*, Vol. 8, No. 1, 1999, pp. 79–87.  
doi:10.1088/0963-0252/8/1/010
- [14] Balkey, M. M., Boivin, R., Kline, J. L., and Scime, E. E., "Ion Heating and Density Production in Helicon Sources near the Lower Hybrid Frequency," *Plasma Sources Science and Technology*, Vol. 10, No. 2, 2001, pp. 284–294.  
doi:10.1088/0963-0252/10/2/318
- [15] Panevsky, M. I., and Bengtson, R. D., "Characterization of the Resonant Electromagnetic Mode in Helicon Discharges," *Physics of Plasmas*, Vol. 11, No. 9, 2004, pp. 4196–4205.  
doi:10.1063/1.1773552
- [16] Tysk, S. M., Denning, C. M., Scharer, J. E., and Akhtar, K., "Optical, Wave Measurements, and Modeling of Helicon Plasmas for a Wide Range of Magnetic Fields," *Physics of Plasmas*, Vol. 11, No. 3, 2004, pp. 878–887.  
doi:10.1063/1.1642656
- [17] Guittienne, P., Chevalier, E., and Hollenstein, C., "Towards an Optimum Antenna for Helicon Waves Excitation," *Journal of Applied Physics*, Vol. 98, No. 8, 2005, p. 083304.  
doi:10.1063/1.2081107
- [18] Degeling, A. W., Jung, C. O., Boswell, R. W., and Ellingboe, A. R., "Plasma Production from Helicon Waves," *Physics of Plasmas*, Vol. 3, No. 7, 1996, pp. 2788–2796.  
doi:10.1063/1.871712
- [19] Kline, J. L., Scime, E. E., Boivin, R. F., Keese, A. M., Sun, X., and Mikhailenko, V. S., "RF Absorption and Ion Heating in Helicon Sources," *Physical Review Letters*, Vol. 88, No. 19, 2002, p. 195002.  
doi:10.1103/PhysRevLett.88.195002
- [20] Krämer, M., Lorenz, B., and Clarenbach, B., "Helicon Sources with  $m = 1$  and  $m = 2$  Helical Antenna Coupling," *Plasma Sources Science and Technology*, Vol. 11, No. 3A, 2002, pp. A120–A130.  
doi:10.1088/0963-0252/11/3A/318
- [21] Wiebold, M., Sung, Y., and Scharer, J. E., "Experimental Observation of Ion Beams in the Madison Helicon Experiment," *Physics of Plasmas*, Vol. 18, No. 6, 2011, p. 063501.  
doi:10.1063/1.3596537
- [22] Lee, C. A., Chen, G., Arefiev, A. V., Bengston, R. D., and Breizman, B. N., "Measurements and Modeling of Radio Frequency Field Structures in a Helicon Plasma," *Physics of Plasmas*, Vol. 18, No. 1, 2011, p. 013501.  
doi:10.1063/1.3533273
- [23] Lemmer, K. M., Gallimore, A. D., and Smith, T. B., "Using a Helicon Source to Simulate Atmospheric Re-Entry Plasma Densities and Temperatures in a Laboratory Setting," *Plasma Sources Science and Technology*, Vol. 18, No. 2, 2009, p. 025019.  
doi:10.1088/0963-0252/18/2/025019
- [24] Toki, K., Shinohara, S., Tanikawa, T., and Shamrai, K. P., "Small Helicon Plasma Source for Electric Propulsion," *Thin Solid Films*, Vols. 506–507, 2006, pp. 597–600.  
doi:10.1016/j.tsf.2005.08.039
- [25] Charles, C., and Boswell, R. B., "Laboratory Evidence of a Supersonic Ion Beam Generated by a Current-Free 'Helicon' Double-Layer," *Physics of Plasmas*, Vol. 11, No. 4, 2004, pp. 1706–1714.  
doi:10.1063/1.1652058
- [26] Charles, C., Boswell, R. W., Alexander, P., Costa, C., Sutherland, O., Pfitzner, L., Franzen, R., Kingwell, J., Parfitt, A., Frigot, P. E., Del Amo, J., and Saccoccia, G., "Operating the Helicon Double-Layer Thruster in a Space Simulation Chamber," *IEEE Transactions on Plasma Science*, Vol. 36, No. 4, 2008, pp. 1196–1197.  
doi:10.1109/TPS.2008.924425
- [27] West, M. D., Charles, C., and Boswell, R. W., "Testing a Helicon Double Layer Thruster Immersed in a Space-Simulation Chamber," *Journal of Propulsion and Power*, Vol. 24, No. 1, 2008, pp. 134–141.  
doi:10.2514/1.131414
- [28] Williams, L. T., and Walker, M. L. R., "Thrust Measurements of a Helicon Plasma Source," *AIAA/ASME/SAE/ASEE Joint Propulsion Conference & Exhibit*, AIAA Paper 2011-5893, 2011.
- [29] Miljakić, D. G., and Chen, F. F., "Density Limit in Helicon Discharges," *Plasma Sources Science and Technology*, Vol. 7, No. 4, 1998, pp. 537–549.  
doi:10.1088/0963-0252/7/4/011
- [30] Goebel, D. M., and Katz, I., *Fundamentals of Electric Propulsion: Ion and Hall Thrusters*, JPL Space Science and Technology Series, Wiley, Hoboken, NJ, 2008, pp. 57, 225.
- [31] Degeling, A. W., Sheridan, T. E., and Boswell, R. W., "Model for Relaxation Oscillations in a Helicon Discharge," *Physics of Plasmas*, Vol. 6, No. 5, 1999, pp. 1641–1648.  
doi:10.1063/1.873419
- [32] Cho, S., "A Self-Consistent Global Model of Neutral Gas Depletion in Pulsed Helicon Plasmas," *Physics of Plasmas*, Vol. 6, No. 1, 1999, pp. 359–364.  
doi:10.1063/1.873289
- [33] Yun, S., Taylor, K., and Tynan, G. R., "Measurement of Radial Neutral Pressure and Plasma Density Profiles in Various Plasma Conditions in Large-Area High-Density Plasma Sources," *Physics of Plasmas*, Vol. 7, No. 8, 2000, pp. 3448–3456.  
doi:10.1063/1.874209
- [34] Fruchtman, A., Makrinich, G., Chabert, P., and Rax, J. M., "Enhanced Plasma Transport Due to Neutral Depletion," *Physical Review Letters*, Vol. 95, No. 11, 2005, p. 115002.  
doi:10.1103/PhysRevLett.95.115002
- [35] Denning, C. M., Wiebold, M., and Scharer, J. E., "Observations of Neutral Depletion and Plasma Acceleration in a Flowing High-Power Argon Helicon Plasma," *Physics of Plasmas*, Vol. 15, No. 7, 2008, p. 072115.  
doi:10.1063/1.2950301
- [36] Houshmandyar, S., and Scime, E. E., "Enhanced Neutral Depletion in a Static Helium Helicon Discharge," *Plasma Sources Science and Technology*, Vol. 21, No. 3, 2012, p. 035008.  
doi:10.1088/0963-0252/21/3/035008
- [37] Sun, X., Biloiu, C., Hardin, R., and Scime, E. E., "Parallel Velocity and Temperature of Argon Ions in an Expanding, Helicon Source Driven Plasma," *Plasma Sources Science and Technology*, Vol. 13, No. 3, 2004, pp. 359–370.  
doi:10.1088/0963-0252/13/3/001
- [38] Tynan, G. R., "Neutral Depletion and Transport Mechanisms in Large-Area High Density Plasma Sources," *Journal of Applied Physics*, Vol. 86, No. 10, 1999, pp. 5356–5364.  
doi:10.1063/1.371532
- [39] Keese, A. M., and Scime, E. E., "Neutral Argon Density Profile Determination by Comparison of Spectroscopic Measurements and a Collisional Radiative Model," *Review of Scientific Instruments*, Vol. 77, No. 10, 2006, p. 10F304.  
doi:10.1063/1.2219440
- [40] Aanesland, A., Liard, L., Leray, G., Jolly, J., and Chabert, P., "Direct Measurements of Neutral Density Depletion by Two-Photon Absorption Laser-Induced Fluorescence Spectroscopy," *Applied Physics Letters*, Vol. 91, No. 12, 2007, p. 121502.  
doi:10.1063/1.2786601
- [41] Shimada, M., Tynan, G. R., and Cattolica, R., "Neutral Gas Density Depletion due to Neutral Gas Heating and Pressure Balance in an Inductively Coupled Plasma," *Plasma Sources Science and Technology*, Vol. 16, No. 1, 2007, pp. 193–199.  
doi:10.1088/0963-0252/16/1/024
- [42] Iordanova, E., de Vries, N., Guillemier, M., and van der Mullen, J. J. A. M., "Absolute Measurements of the Continuum Radiation to Determine the Electron Density in a Microwave-Induced Argon Plasma," *Journal of Physics D: Applied Physics*, Vol. 41, No. 1, 2008, p. 015208.  
doi:10.1088/0022-3727/41/1/015208
- [43] Oh, D. Y., and Hastings, D. E., "Experimental Verification of a PIC-DSMC Model for Hall Thruster Plumes," *AIAA/ASME/SAE/*

- ASEE Joint Propulsion Conference and Exhibit, AIAA Paper 96-3196, 1996.
- [44] Boyd, I. D., "Computation of the Plume of an Anode-Layer Hall Thruster," *Journal of Propulsion and Power*, Vol. 16, No. 5, 2000, pp. 902–909.  
doi:10.2514/2.5658
- [45] Boyd, I. D., "Numerical Simulation of Hall Thruster Plasma Plumes in Space," *IEEE Transactions on Plasma Science*, Vol. 34, No. 5, 2006, pp. 2140–2147.  
doi:10.1109/TPS.2006.879096
- [46] Choi, Y., Keidar, M., and Boyd, I. D., "Particle Simulation of Plume Flows from an Anode-Layer Hall Thruster," *Journal of Propulsion and Power*, Vol. 24, No. 3, 2008, pp. 554–561.  
doi:10.2514/1.28384
- [47] Passaro, A., Vicini, A., Nania, F., and Biagioni, L., "Numerical Rebuilding of SMART-1 Hall Effect Thruster Plasma Plume," *Journal of Propulsion and Power*, Vol. 26, No. 1, 2010, pp. 149–158.  
doi:10.2514/1.36821
- [48] Bird, G. A., *Molecular Gas Dynamics and the Direct Simulation of Gas Flows*, Oxford Univ. Press, Oxford, England, U.K., 1994.
- [49] Birdsall, C. K., and Langdon, A. B., *Plasma Physics via Computer Simulation*, Adam Hilger, Bristol, England, U.K., 1991.
- [50] Boyd, I. D., Van Gilder, D. B., and Liu, X., "Monte Carlo Simulation of Neutral Xenon Flows in Electric Propulsion Devices," *Journal of Propulsion and Power*, Vol. 14, No. 6, 1998, pp. 1009–1015.  
doi:10.2514/2.5366
- [51] Walker, M. L. R., Gallimore, A. D., Boyd, I. D., and Chai, C., "Vacuum Chamber Pressure Maps of a Hall-Thruster Cold Flow Expansion," *Journal of Propulsion and Power*, Vol. 20, No. 6, 2004, pp. 1127–1131.  
doi:10.2514/1.8973
- [52] Bird, G. A., "DS2V User's Manual: Visual DSMC Program for Two-Dimensional and Axially Symmetric Flows," <http://gab.com.au> [retrieved 10 Nov. 2012].

L. King  
Associate Editor